Accurate Characterization of the Pore Volume in Microporous Crystalline Materials

Daniele Ongari,[†] Peter G. Boyd,[†] Senja Barthel,[†] Matthew Witman,[‡] Maciej Haranczyk,[¶,§] and Berend Smit[*,†]

Laboratory of Molecular Simulation, Institut des Sciences et Ingeénierie Chimiques, Ecole Polytechnique Fédérale de Lausanne (EPFL), Rue de l'Industrie 17, CH-1951 Sion, Valais, Switzerland, Department of Chemical and Biomolecular Engineering, University of California, Berkeley 94760, U.S.A., IMDEA Materials Institute, C/Eric Kandel 2, 28906 Getafe, Madrid, Spain, and Computational Research Division, Lawrence Berkeley National Laboratory, Berkeley, California 94720, USA

E-mail: berend.smit@epfl.ch

[*]To whom correspondence should be addressed
[†]EPFL Sion
[‡]Berkeley
[¶]IMDEA
[§]Berkeley Nat. Lab.

Three-Dimensional Pore Models

Three simple pore models (spherical shell, cylindrical shell, and reticular) are presented in the manuscript to demonstrate how the He void fraction relates to the geometric pore volume. For He interactions inside the spherical and cylindrical shell pores, the analytical model is derived in the following subsections. The He adsorbate interacts with the pore wall atoms via a Lennard-Jones potential (see Eqn. 1); however, rather than interacting with discrete atomic centers in the pore wall, the interaction is uniformly smeared across the pore surface which permits an analytical expression that can be directly integrated (rather than requiring a simulation) to obtain a value for the He void fraction (θ_{He}). To use this smeared potential, the surface density of atoms in the spherical and cylindrical shell pore models is specified to be $\eta = 1$ atom $/[\pi * (1.2\text{Å})^2]$. This value is slightly higher than the surface density of carbon atoms in graphene to account for favorable dispersion interactions that would exist in a real porous material that usually contains atoms beyond the pore wall and are not accounted for in a pore shell model. In the reticular model, the framework consists of simple rods on the edges of a cube. Hence we now specify a line (rather than surface) density of carbon atoms ($\eta = 1$ atom $/1.2$Å) to uniformly smear the interactions of the He with the rods of the reticular framework model.

The interaction energy between He and a framework atom with discrete spacial coordinates follows from the Lennard Jones potential, which depends on the interatomic separation d and the model parameters ϵ_{ij} and σ_{ij}.

$$U_{ij}(d) = 4\epsilon_{ij}\left[\left(\frac{\sigma_{ij}}{d}\right)^{12} - \left(\frac{\sigma_{ij}}{d}\right)^{6}\right] \tag{1}$$

In the following subsections it will be shown how this potential can be uniformly smeared across the pore wall atoms. The epsilon and sigma parameters for the carbon atoms in the pore walls for all the analytical models are taken from UFF,[1] while the epsilon and sigma parameters for He are taken from Hirschfelder *et al.*[2] The mixing parameters are determined

by Lorentz-Berthelot mixing rules.

Spherical shell pore model

We consider a spherical shell pore model with radius R_p. The adsorption energy of one Helium atom within the spherical pore is dependent only on the r coordinate due to spherical symmetry. However to determine this energy requires an integration of the host/adsorbate interaction across the smeared surface. First, we must define the distance between the adsorbate and any point on the pore surface, given by d_w in Eqn 2.

$$d_w(r, \phi, R_p) = \sqrt{R_p^2 + r^2 - 2R_p r cos(\phi)} \tag{2}$$

When the He interactions with the pore atoms are smeared across the pore shell surface rather than computed by discrete pairwise interactions, the total adsorption energy can be expressed by the integral in Eqn 3, where $U_{tot,1}$ represents the adsorption energy per pore wall atom. The total energy with all the atoms in the pore wall is then obtained by simply multiplying by the surface density of pore atoms, η, in Eqn 4, where U_{tot} is the total adsorption energy.

$$U_{tot,1}(r, R_p) = \int_0^{2\pi} d\theta \int_0^{\pi} d\phi \; R_p^2 sin(\phi) 4\epsilon_{ij} \left[\left(\frac{\sigma_{ij}}{d_w(r, \phi, R_p)} \right)^{12} - \left(\frac{\sigma_{ij}}{d_w(r, \phi, R_p)} \right)^{6} \right] \tag{3}$$

$$U_{tot}(r, R_p) = 2\pi\eta R_p^2 \int_0^{\pi} d\phi \; sin(\phi) 4\epsilon_{ij} \left[\left(\frac{\sigma_{ij}}{d_w(r, \phi, R_p)} \right)^{12} - \left(\frac{\sigma_{ij}}{d_w(r, \phi, R_p)} \right)^{6} \right] \tag{4}$$

Next, the He void fraction is defined by:

$$\theta_{He} = \frac{1}{V} \int dV \; exp(-\beta U_{tot}) \tag{5}$$

which for the spherical pore model is expressed by Eqn 6.

$$\theta_{He}(R_p) = \frac{4\pi}{V_p} \int_0^{R_p} dr\, r^2 exp(-\beta U_{tot}(r, R_p)) \tag{6}$$

This expression is numerically integrated to obtain the exact **He** void fraction for the spherical pore model. The geometric void fraction for the comparison is computed as:

$$\theta_{Gm}(R_p) = \frac{\frac{4}{3}\pi(R_p - \sigma_{ii})^3}{V_p} \tag{7}$$

with σ_{ii} being the Lennard-Jones sigma parameter for carbon.

Cylindrical shell pore model

We consider a cylindrical shell pore model with radius R_{cyl} and axial length $2z_0$. Again due to symmetry, the adsorption energy of He is only dependent on its radial coordinate since the cylinder is axially uniform. The slight difference between the spherical model is that the distance between the adsorbate and the pore wall in the axial direction must be considered.

$$d_w(r, \theta, R_{cyl}) = \sqrt{R_{cyl}^2 + r^2 - 2R_{cyl} r cos(\theta) + z^2} \tag{8}$$

Thus the expression for the total adsorbate energy is given by Eqn 9, where the cylinder is truncated such that the axial length is 2 times the cutoff radius ($2z_0 = 25$ Å).

$$U_{tot}(r, R_{cyl}) = \eta \int_{-z_0}^{z_0} dz \int_0^{2\pi} d\theta\, R_{cyl} 4\epsilon_{ij} \left[\left(\frac{\sigma_{ij}}{d_w(r, \theta, R_{cyl})} \right)^{12} - \left(\frac{\sigma_{ij}}{d_w(r, \theta, R_{cyl})} \right)^{6} \right] \tag{9}$$

Extrapolation of 5 to the cylindrical pore model yields Eqn 10.

$$\theta_{He}(R_{cyl}) = \frac{(2\pi)(2z_0)}{V_{cyl}} \int_0^{R_{cyl}} dr\, r \cdot exp(-\beta U_{tot}(r, R_{cyl})) \tag{10}$$

The geometric void fraction for the comparison is computed as:

$$\theta_{Gm}(R_{cyl}) = \frac{2z_0\pi(R_p - \sigma_{ii})^2}{V_{cyl}} \tag{11}$$

with σ_{ii} being the Lennard-Jones sigma parameter for carbon.

Reticular framework model

For the reticular model, the convergence of the numerical integration of the closed form expression for the He void fraction was poor. Thus we did not use the same numerical integration approach as the previous two examples. Specifically, the rods in the reticular structure were built from equispaced carbon "dummy" atoms on the edges of a cube, and these equispaced dummy atoms had a uniform separation distance of d_{bin}=0.2 Å (Figure S1). The σ_{ij} interaction parameter between the carbon dummy atom and the He adsorbate remained unchanged, but the ϵ^*_{ij} interaction was modified as follows:

$$\epsilon^*_{ij} = \epsilon_{ij}\frac{d_{ii}}{d_{bin}} \tag{12}$$

with d_{ii}=1.2 Å to enforce the line density to be coherent with the surface density in the previous models. Hence there are six dummy beads per 1.2 Å, with each contributing a proportional fraction of the dispersion energy of a single carbon atom. This approximates the smearing utilized in the previous two examples and then the He void fraction is calculated directly from a simulation rather than a numerical integration.

The helium void fraction was computed using the Raspa package[3] by performing Widom insertions for 10,000 sample points. The value for the void fraction was ensured to converge within 1%. The geometric void fraction was computed with the Zeo++ package, using 100,000 sample points and assuming the dummy atoms as rigid spheres with a diameter of σ_{ii}, the Lennard-Jones sigma parameter for carbon.

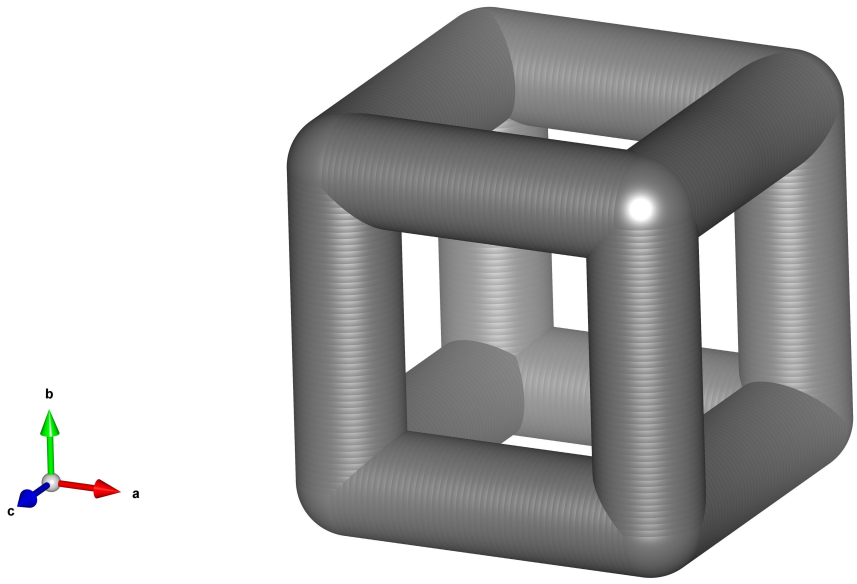

Figure S1: Representation of the reticular framework model. Carbon "dummy" atoms are represented by gray spheres.

Experimental Values for the Void Fraction

Table S1: The frameworks presented in the section "Comparison With Experimental Data for 10 MOFs" are listed, referring to the work in which the pore volume has been computed.

Name	CSD refcode	Ref.
SNU-50	ALAMUW	[4]
UTSA-62	BICPUA	[5]
DUT-13	EHIJAH	[6]
HKUST-1	FIQCEN	[7]
UTSA-34	HANWAW	[8]
PCN-46	LUYHAP	[9]
UTSA-20	ONIXOZ	[10]
NU-125	REWNEO	[11]
SNU-30	VAGMAT	[12]
PCN-6A	VUJBIM	[13]

Evidence of flexibility in the framework was found in DUT-13 and SNU-30. While for DUT-13 the accessible probe occupiable volume agrees with the experimental value (with an error within the 5% of the void fraction), for SNU-30 the experimental value for the pore volume is considerably lower than the computed one. This reveals the state of the framework when nitrogen molecules are filling the pores (open pores in DUT-13 and shrunken in SNU-30) and when the X-ray data were collected to refine the crystallographic structure we used for the calculation (open pores in both the cases).

Lennard-Jones Parameters

Helium parameters from Hirschfelder *et al.*:[2]

Atom	σ **(Å)**	ϵ/k_b **(K)**
He	2.64	10.9

Parameters for the other atoms from UFF:[1]

Atom	σ **(Å)**	ϵ/k_b **(K)**
H	2.571	22.144
Li	2.184	12.582
Be	2.446	42.778
B	3.638	90.589
C	3.431	52.843
N	3.261	34.726
O	3.118	30.196
F	2.997	25.164
Ne	2.889	21.137
Na	2.658	15.098
Mg	2.691	55.863
Al	4.008	254.152
Si	3.826	202.315
P	3.695	153.498
S	3.595	137.896
Cl	3.516	114.243
Ar	3.446	93.105
K	3.396	17.614
Ca	3.028	119.779
Sc	2.936	9.562
Ti	2.829	8.556
V	2.801	8.052
Cr	2.693	7.549
Mn	2.638	6.543
Fe	2.594	6.543
Co	2.559	7.046
Ni	2.525	7.549
Cu	3.114	2.516
Zn	2.462	62.406

Atom	σ **(Å)**	ϵ/k_b **(K)**
Ga	3.905	208.858
Ge	3.813	190.74
As	3.769	155.511
Se	3.746	146.452
Br	3.732	126.321
Kr	3.689	110.72
Rb	3.665	20.131
Sr	3.244	118.269
Y	2.98	36.236
Zr	2.783	34.726
Nb	2.82	29.693
Mo	2.719	28.183
Tc	2.671	24.157
Ru	2.64	28.183
Rh	2.609	26.673
Pd	2.583	24.157
Ag	2.805	18.118
Cd	2.537	114.746
In	3.976	301.459
Sn	3.913	285.355
Sb	3.938	225.969
Te	3.982	200.302
I	4.009	170.609
Xe	3.924	167.086
Cs	4.024	22.647
Ba	3.299	183.191
La	3.138	8.556
Ce	3.168	6.543
Pr	3.213	5.033
Nd	3.185	5.033
Pm	3.16	4.529
Sm	3.136	4.026
Eu	3.112	4.026
Gd	3.001	4.529
Tb	3.074	3.523
Dy	3.054	3.523
Ho	3.037	3.523

Atom	σ **(Å)**	ϵ/k_b **(K)**
Er	3.021	3.523
Tm	3.006	3.02
Yb	2.989	114.746
Lu	3.243	20.634
Re	2.632	33.216
Os	2.78	18.621
Ir	2.53	36.739
Pt	2.454	40.262
Au	2.934	19.628
Hg	2.41	193.759
Tl	3.873	342.224
Pb	3.828	333.669
Bi	3.893	260.695
Po	4.195	163.563
At	4.232	142.929
Rn	4.245	124.811
Fr	4.365	25.164
Ra	3.276	203.322
Ac	3.099	16.608
Th	3.025	13.085
Pa	3.05	11.072
U	3.025	11.072
Np	3.05	9.562
Pu	3.05	8.052
Am	3.012	7.046
Cm	2.963	6.543
Bk	2.975	6.543
Cf	2.952	6.543
Es	2.939	6.039
Fm	2.927	6.039
Md	2.917	5.536
No	2.894	5.536
Lr	2.883	5.536
Hf	2.798	36.236
Ta	2.824	40.765
W	2.734	33.719

Assessment of the convergence in the 3D model

Table S2: Assessment of the different volume fractions in the three-dimentional model of Figure 5, for an increasing number of sample points per cubic angstrom.

Ac-PC	NAc-PC	Ac-PO	NAc-PO	Narrow	Overlap	N	N/Å^3
0.0060	0.0060	0.0100	0.0080	0.0380	0.9440	1000	0.13
0.0070	0.0046	0.0184	0.0120	0.0230	0.9466	5000	0.67
0.0086	0.0042	0.0245	0.0120	0.0148	0.9487	10000	1.35
0.0079	0.0051	0.0257	0.0150	0.0122	0.9472	25000	3.37
0.0077	0.0048	0.0271	0.0158	0.0092	0.9480	50000	6.73
0.0080	0.0051	0.0277	0.0168	0.0085	0.9470	75000	10.10
0.0079	0.0053	0.0277	0.0170	0.0080	0.9473	100000	13.47
0.0076	0.0052	0.0279	0.0170	0.0071	0.9479	200000	26.94
0.0074	0.0052	0.0279	0.0170	0.0069	0.9483	300000	40.41
0.0075	0.0052	0.0282	0.0171	0.0067	0.9480	400000	53.88
0.0074	0.0053	0.0282	0.0173	0.0066	0.9480	500000	67.35

Pore volume calculation in other programs

We describe and assess the pore volume calculation in two other softwares: BOVIA Materials Studio (Accelrys Software Inc., San Diego, CA) and MOFomics.[14]

BOVIA Material Studio is a commercial software package, and it is able to compute the probe occupiable pore volume by using the Connolly algorithm. This algorithm decomposes the framework (or generally, a molecule) in a set of convex, saddle and concave pieces, whose volume is analytically computed and summed to obtain the solvent-free volume.[15] The total probe occupiable pore volume is therefore given by the total volume of the unit cell minus the solvent-free volume. The value of the void fraction obtained for the benchmark framework HKUST-1 (CSD code: FIQCEN) is 0.681. This value is very close to both the experimental value and the probe occupiable void fraction computed with our algorithm (considering that Material Studio is using a different set of values for the atomic radii than UFF's sigma).

MOFomics is an online platform to upload, analyse and store MOF structures. The algorithm used to compute the pore volume is different from the methods described in this work. The porous network is decomposed into a set of cylinders and spheres and the internal

volume of these is taken as the total pore volume.[16] Accessible pore volume is evaluated by considering only the cylinders and spheres that are accessible to a probe of specific radii: 1, 2, 3 and 4 Å.

References

(1) Rappé, A. K.; Casewit, C. J.; Colwell, K.; Goddard, W. A.; Skiff, W. UFF, a full periodic table force field for molecular mechanics and molecular dynamics simulations. *J. Am. Chem. Soc.* **1992**, *114*, 10024–10035.

(2) Hirschfelder, J.; Bird, R. B.; Curtiss, C. F. Molecular theory of gases and liquids. **1964**,

(3) Dubbeldam, D.; Calero, S.; Ellis, D.; Snurr, R. RASPA 2.0: Molecular software package for adsorption and diffusion in (flexible) nanoporous materials. *Mol. Simul.* **2016**, *42*, 81–101.

(4) Prasad, T. K.; Hong, D. H.; Suh, M. P. High gas sorption and metal-ion exchange of microporous metal–organic frameworks with incorporated imide groups. *Chem. Eur. J.* **2010**, *16*, 14043–14050.

(5) He, Y.; Furukawa, H.; Wu, C.; O'Keeffe, M.; Krishna, R.; Chen, B. Low-energy regeneration and high productivity in a lanthanide–hexacarboxylate framework for high-pressure CO 2–CH 4–H 2 separation. *Chem. Comm.* **2013**, *49*, 6773–6775.

(6) Grünker, R.; Senkovska, I.; Biedermann, R.; Klein, N.; Lohe, M. R.; Müller, P.; Kaskel, S. A highly porous flexible metal–organic framework with corundum topology. *Chem. Comm.* **2011**, *47*, 490–492.

(7) Mason, J. A.; Veenstra, M.; Long, J. R. Evaluating metal–organic frameworks for natural gas storage. *Chem. Sci.* **2014**, *5*, 32–51.

(8) He, Y.; Zhang, Z.; Xiang, S.; Wu, H.; Fronczek, F. R.; Zhou, W.; Krishna, R.; O'Keeffe, M.; Chen, B. High separation capacity and selectivity of C2 hydrocarbons over methane within a microporous metal–organic framework at room temperature. *Chem. Eur. J.* **2012**, *18*, 1901–1904.

(9) Zhao, D.; Yuan, D.; Yakovenko, A.; Zhou, H.-C. A NbO-type metal–organic framework derived from a polyyne-coupled di-isophthalate linker formed in situ. *Chem. Comm.* **2010**, *46*, 4196–4198.

(10) Guo, Z.; Wu, H.; Srinivas, G.; Zhou, Y.; Xiang, S.; Chen, Z.; Yang, Y.; Zhou, W.; O'Keeffe, M.; Chen, B. A metal–organic framework with optimized open metal sites and pore spaces for high methane storage at room temperature. *Angew. Chem., Int. Ed.* **2011**, *50*, 3178–3181.

(11) Wilmer, C. E.; Farha, O. K.; Yildirim, T.; Eryazici, I.; Krungleviciute, V.; Sarjeant, A. A.; Snurr, R. Q.; Hupp, J. T. Gram-scale, high-yield synthesis of a robust metal–organic framework for storing methane and other gases. *Energy Environ. Sci.* **2013**, *6*, 1158–1163.

(12) Park, H. J.; Cheon, Y. E.; Suh, M. P. Post-synthetic reversible incorporation of organic linkers into porous metal–organic frameworks through single-crystal-to-single-crystal transformations and Modification of Gas-Sorption Properties. *Chem. Eur. J.* **2010**, *16*, 11662–11669.

(13) Yuan, D.; Zhao, D.; Sun, D.; Zhou, H.-C. An isoreticular series of metal–organic frameworks with dendritic hexacarboxylate ligands and exceptionally high gas-uptake capacity. *Angew. Chem., Int. Ed.* **2010**, *49*, 5357–5361.

(14) First, E. L.; Floudas, C. A. MOFomics: Computational pore characterization of metal–organic frameworks. *Microporous Mesoporous Mater.* **2013**, *165*, 32–39.

(15) Connolly, M. L. Computation of molecular volume. *J. Am. Chem. Soc.* **1985**, *107*, 1118–1124.

(16) First, E. L.; Gounaris, C. E.; Wei, J.; Floudas, C. A. Computational characterization of zeolite porous networks: an automated approach. *Phys. Chem. Chem. Phys.* **2011**, *13*, 17339–17358.